CELL BIOLOGY

Signal recognition particle receptor-β (SR-β) coordinates cotranslational N-glycosylation

Chatchai Phoomak[1,2], Natalie Rinis[1], Marta Baro[1], Shiteshu Shrimal[3], Daniel Bennett[1], Scott A. Shaffer[3,4], Mark Lehrman[5], Reid Gilmore[3], Joseph N. Contessa[1,6]*

Proteins destined for the secretory compartment of the cell are cotranslationally translocated into the endoplasmic reticulum. The majority of these proteins are N-glycosylated, a co- and posttranslational modification that ensures proper protein folding, stability, solubility, and cellular localization. Here, we show that the β subunit of the signal recognition particle receptor (SR) is required for assembly of the N-glycosylation–competent translocon. We report that guanine analog chemical probes identified by high-throughput screening or mutation of the SR-β guanosine triphosphate binding site cause an N-glycosylation–deficient phenotype. Neither method alters the association of SR-α with SR-β, but both approaches reduce the association of SR-β with the oligosaccharyltransferase complex. These experiments demonstrate that SR-β has a previously unrecognized function coordinating endoplasmic reticulum translation with N-glycosylation.

INTRODUCTION

Asparagine (N)–glycosylation is a protein modification conserved across the three domains of life and enzymatically catalyzed by oligosaccharyltransferase (OST). N-glycosylation occurs co- and posttranslationally in the endoplasmic reticulum (ER) of eukaryotes, where it facilitates protein folding and stability (*1*). In metazoans, the number of N-glycosylation sites has increased substantially and is accompanied by expansion of the cellular machinery for both N-glycan transfer and ribosome targeting to the ER. Recently, cryo–electron microscopy analyses have advanced mechanistic insights for the assembly of multiprotein complexes required for cotranslational N-glycosylation. These studies have isolated either an early translocon unassociated prehandover complex composed of the ribosome and nascent chain (RNC), the signal recognition particle (SRP), and a truncated SRP receptor (SR) (*2*, *3*) or the membrane-embedded RNC-translocon-OST supercomplex (*4*, *5*). However, an understanding of the transition between these states has remained elusive.

Although N-glycosylation requires more than 45 genes for synthesis and transfer of lipid-linked oligosaccharide (LLO) precursors to newly synthesized proteins (*6*), few targeted pharmacologic agents that alter this biosynthetic process have been discovered. This limits strategies for probing the functions of these gene products and uncovering the biologic effects of target inhibition. To date, only two classes of inhibitors have been found. The first are tunicamycin natural products that are produced by *Streptomyces* bacteria and block the function of DPAGT1 (*7*). Tunicamycin eliminates all LLO synthesis, blocks all N-glycosylation, and has largely been used as a pharmacologic tool to induce ER stress. The second is a class of benzamido-aminothiazole analogs that partially block activity of the OST catalytic subunits (*8*). These inhibitors enable the investigation of incomplete inhibition of N-glycosylation for the first time and have led to ongoing development of these inhibitors as potential antitumor or antiviral agents. Here, we report thioguanine analogs to be a third class of N-glycosylation inhibitors. These chemical probes alter assembly dynamics of the OST with the RNC-SR complex, revealing a previously unknown mechanism for regulation of N-glycosylation.

RESULTS

High-throughput screens identify 6-TG as an N-glycosylation inhibitor

In an effort to identify additional small-molecule probes that disrupt N-glycosylation, we analyzed pooled data from a phenotypic high-throughput screening (HTS) program measuring glycan site occupancy as a readout (Fig. 1A). Of the 361,103 small molecules screened, three purine related analogs, initially unconfirmed in tertiary assays (*8*, *9*), were tested in a redesigned, low-throughput orthogonal assay that reports molecular weight size changes of a glycosylated Halo protein (Halo3N) on Western blot (*10*). These experiments demonstrated weak inhibition of N-glycosylation, guiding further analog testing and ultimately identification of 6-thioguanine (6-TG; Fig. 1B) as a potent and dose-dependent inhibitor that reduced N-glycosylation in multiple cell lines (fig. S1, A and B). Through comparative testing with 6-mercaptopurine (6-MP) and 2-aminopurine (2-AP), a structure-activity relationship indicating the requirements for the thiol and amino groups was established (Fig. 1B). The time course for inhibition of ~6 hours, between that of DPAGT1 inhibition with tunicamycin and OST inhibition with NGI-1, indicated that 6-TG could either target an intermediate step in glycan synthesis or be metabolized by the cell to an active form. Analysis of LLO in control or 6-TG–treated samples showed an enrichment of the mature 14-carbohydrate glycan precursor (Fig. 1C). This result excludes the possibility that 6-TG significantly alters glycan precursor biosynthesis, and a reduction of N-glycosylation concurrent with reduced LLO turnover instead

[1]Department of Therapeutic Radiology, Yale School of Medicine, New Haven, CT 06511, USA. [2]Department of Biology, Faculty of Science, Chulalongkorn University, Bangkok 10330, Thailand. [3]Department of Biochemistry and Biotechnology, University of Massachusetts Chan Medical School, Worcester, MA 01605, USA. [4]Mass Spectrometry Facility, University of Massachusetts Chan Medical School, Shrewsbury, MA 01545, USA. [5]Department of Pharmacology, UT Southwestern Medical Center at Dallas, 6001 Forest Park Rd., Dallas, TX 75390, USA. [6]Department of Pharmacology, Yale School of Medicine, New Haven, CT 06511, USA.
*Corresponding author: Email: joseph.contessa@yale.edu

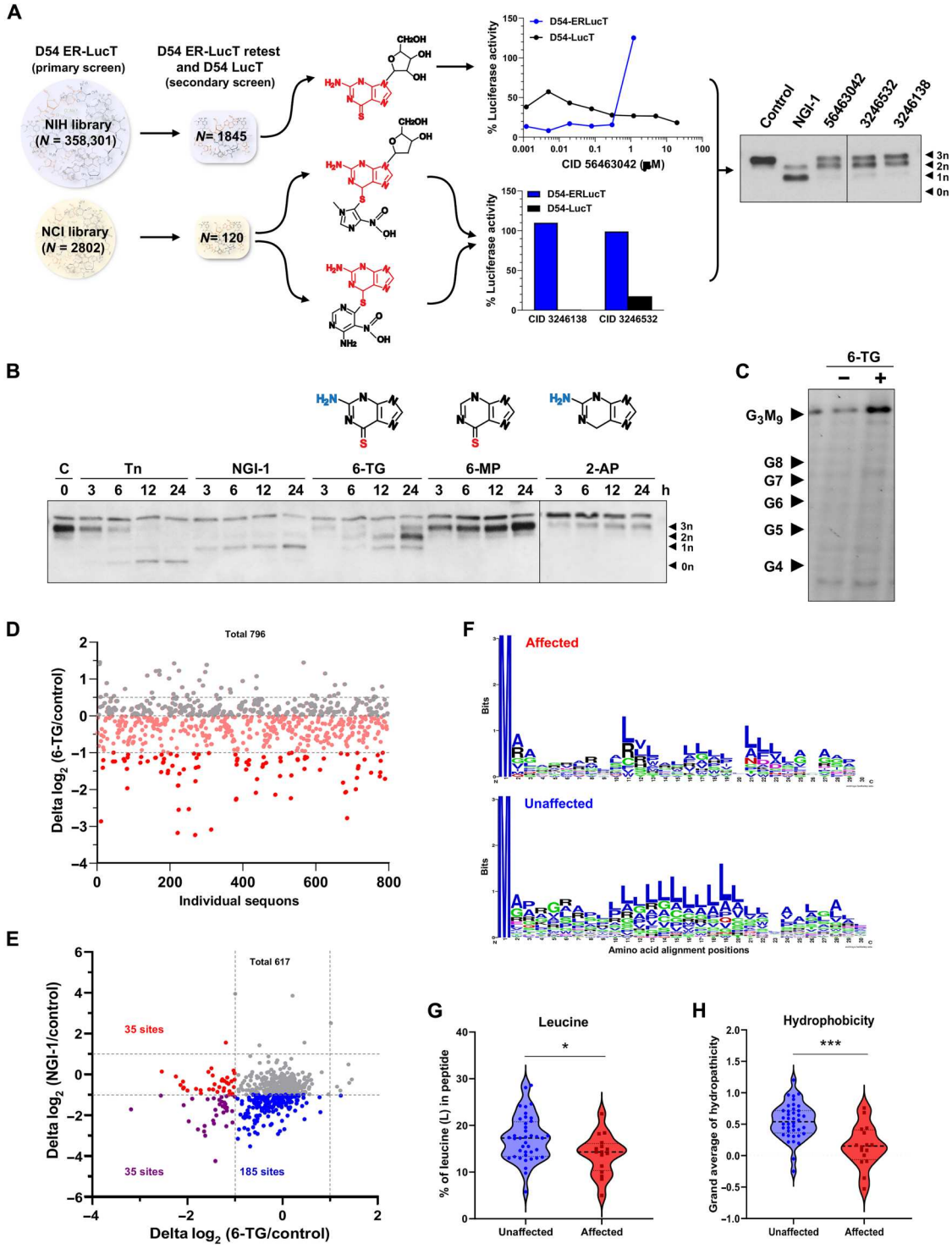

Fig. 1. HTS and quantitative glycoproteomics identify 6-TG as an N-glycosylation inhibitor. (**A**) Results of two chemical library screens that identified purine-related (in red) analogs with N-glycosylation inhibitory activity in primary (ER-LucT) but not secondary false-positive (LucT) cell-based assays. Biologic activity was confirmed by Halo3N size shifts seen by Western blot. (**B**) Structure-activity relationships for purine analogs demonstrating loss of activity without sulfur or amine substituents. The cells were treated with 1 μM tunicamycin (Tn), 10 μM NGI-1, 10 μM 6-TG, 10 μM 6-MP, or 10 μM 2-AP for 3, 6, 12, and 24 hours, and results are representative of three experiments. (**C**) FACE analysis of LLOs treated with 6-TG representative of two biologically independent samples. G_3M_9 indicates the mature LLO size. (**D**) N-glycan site occupancy for 796 individual sequons in control versus 6-TG–treated samples. Data points represent the $\Delta\log_2$ change average of four independent experiments. (**E**) Site occupancy of 617 individual sequons identified from either 10 μM NGI-1 or 10 μM 6-TG treatment. (**F**) Leader peptide consensus sequences for the first 30 amino acids of 6-TG affected versus unaffected proteins determined by WebLogo analysis. (**G**) Hydrophobicity and (**H**) leucine content of leader peptides determined with Sequence Manipulation Suite and ProtParam (*P < 0.05 and ***P < 0.001, t test)

provides biochemical evidence that 6-TG disrupts glycosylation per se.

Glycoproteomics identify site-specific inhibition of N-glycosylation

To characterize N-glycosylation sequons with reduced site occupancy following 6-TG treatment, we performed quantitative glycoproteomic analysis using stable isotope labeling by amino acids in cell culture (SILAC) as previously described (*11*). Of 796 acceptor sequons identified, 6-TG reduced average glycan site occupancy by >25% on 244 sites and by >50% on 95 sites, verifying that inhibition is widespread across the N-glycoproteome (Fig. 1D and table S1). Comparison to a small dataset of sequons affected by OST inhibition with NGI-1 (*8*) suggested only partial overlap, and formal comparison following parallel quantitation of NGI-1's effects using SILAC confirmed that 6-TG and NGI-1 preferentially reduce N-glycosylation for different sequons (Fig. 1E and table S2). Of the 617 sequons with site occupancy quantification in both the 6-TG and NGI-1 datasets, only 50% of sites with $\Delta\log_2 < -1.0$ after 6-TG treatment were similarly sensitive to NGI-1. Conversely, only 16% of sequons with $\Delta\log_2 < -1.0$ after NGI-1 treatment were sensitive to 6-TG. To further understand these differences, sequons were divided into NXT and NXS/C groups and ranked by $\Delta\log_2$ values. For NGI-1, these lines intersect (fig. S1C), indicating a greater effect on NXS/C sequons, and demonstrate an identical pattern seen from knockout (KO) of the STT3A or STT3B catalytic subunits of the OST (*11*). In contrast, plotting of NXT and NXS/C groups shows no intersection for 6-TG–treated samples (fig. S1D). In addition, comparison of occupancy for sequons with $\Delta\log_2 > 2.0$ from NGI-1– versus 6-TG–treated samples (fig. S1E) illustrates that, unlike pharmacologic or genetic inhibition of the OST, NXS/C sites are not more susceptible to 6-TG treatment. These experiments at the level of the glycoproteome indicate that 6-TG has a separate mechanism for inhibiting N-glycosylation and a pharmacologic target that is distinct from the OST.

Because no pattern for affected versus unaffected sequons could be identified, we questioned whether the drug's effect could be dependent on characteristics of the protein instead of features of individual sequons. To classify proteins as affected versus unaffected, we analyzed proteins with more than one quantified sequon. Those with at least one sequon having a $\Delta\log_2$ value between 0 and 0.5 (fig. S1F) were categorized as unaffected, and those with at least one quantified sequon having $\Delta\log_2$ values < -1.0 (fig. S1G) were categorized as affected. Central plots in fig. S1 (F and G) illustrate these unaffected or affected proteins, respectively. The uppermost plots show values for all other sequons quantified in these unaffected versus affected protein categories, and the lower plots (gray) represent all quantified sequons in the dataset. Comparison of these groups demonstrated a trend for individual proteins to be either unaffected or affected by 6-TG treatment. Site occupancy for each of the 164 sequons from the 56 proteins with N-terminal signal sequences (table S3; $n = 40$ unaffected and $n = 16$ affected) is presented in fig. S1H, and a comparison of these signal sequences demonstrated significant sequence diversity between the affected and unaffected groups (Fig. 1F). Affected proteins have signal sequences with a lower leucine content (Fig. 1G) and less hydrophobicity overall (Fig. 1H). These data suggest that 6-TG's target could alter the dynamics of signal sequence handover and coordination of N-glycosylation at the translocon.

CRISPR-Cas9 pooled genetic screening for 6-TG target discovery

A strategy to identify 6-TG's molecular target was designed using the ER-translated Halo1N reporter protein (*6*), which covalently binds its fluorescent ligand only when Halo N-glycosylation is absent. 6-TG potently blocks Halo1N glycosylation, causing treated cells to become fluorescent upon Halo ligand exposure (Fig. 2A). We therefore reasoned that genes required for 6-TG's activity could be identified by fluorescence-activated cell sorting (FACS) analysis for loss of function/fluorescence, with selection of the nonfluorescent population of cells (Fig. 2B). A549-Halo1N-Cas9 cells were therefore screened under control or 6-TG treatment conditions using a whole-genome guide RNA (gRNA) library, followed by selection of the ~2% of nonfluorescent cells in three biologically independent replicates. Deep sequencing results of 6-TG–treated, nonfluorescent cells were compared to those from the unsorted but gRNA library–infected population (table S4) and then analyzed for significant gRNA enrichment or depletion using MAGeCK analysis (table S5). We found that gRNAs for HPRT1 and NUDT5, enzymes required for conversion of 6-TG to 6-TGTP, were enriched ($q < 0.003$ for both; Fig. 2C). Identification of these gene products is consistent with the time course studies (Fig. 1B) that suggest a requirement for converting 6-TG to an active metabolite. KO of HPRT1 (*12*) confirmed that it is necessary for 6-TG activity (fig. S2A). Enrichment for STT3A (but not STT3B) gRNAs led to experiments showing that 6-TG's activity is partially reduced with STT3A KO (fig. S2B). This result indicates that STT3A is not the direct target of 6-TG but is likely to be involved in the mechanism of action. Because STT3A-containing (but not STT3B-containing) OST complexes associate with the translocon, these data also suggested that 6-TG could be altering cotranslational N-glycosylation.

KO or knockdown of other potential targets including the ER protein FNDC3B, the glycosyltransferase ALG12, and the ER-associated degradation-linked E2 ubiquitin conjugating enzyme UBE2J1 had no effect on 6-TG activity (fig. S2, C to F). One possibility is that KO of these proteins modifies 6-TG's activity but that cells undergo rapid adaptation, an outcome we have previously observed while characterizing the role of the TRAP complex in mediating N-glycosylation (*6*). gRNAs for the TSC2 tumor suppressor were significantly depleted ($q < 0.003$), and TSC1 was ranked as the fourth highest gene for negative enrichment (table S5). TSC1/TSC2 negatively regulates ribosome translation via mechanistic target of rapamycin (mTOR) control (*13*), implying that increased translation enhances 6-TG's inhibitory effect on N-glycosylation. In agreement with this hypothesis, inhibition of mTOR with structurally unrelated inhibitors, INK128 or rapamycin, reduced the effects of 6-TG on N-glycosylation for both the Halo1N reporter and endogenously expressed gp130 (Fig. 2D) but did not reverse the effects of an OST inhibitor on N-glycosylation (fig. S2G). The rescue of the hypoglycosylation phenotype by mTOR inhibition mechanistically places the target of 6-TG between the ribosome and the OST. Furthermore, a link to ribosome function was also inferred by screen depletion of gRNAs for UFC1, an E2-like enzyme subunit required for UFMylation, a protein modification that primarily targets the ribosomal protein L26 (*14*). Together, these data led us to consider the possibility that a protein unknown to play a role in regulating N-glycosylation, and beyond the established RNC-translocon-OST complex (*4*, *5*), is the target for 6-TG–dependent inhibition of

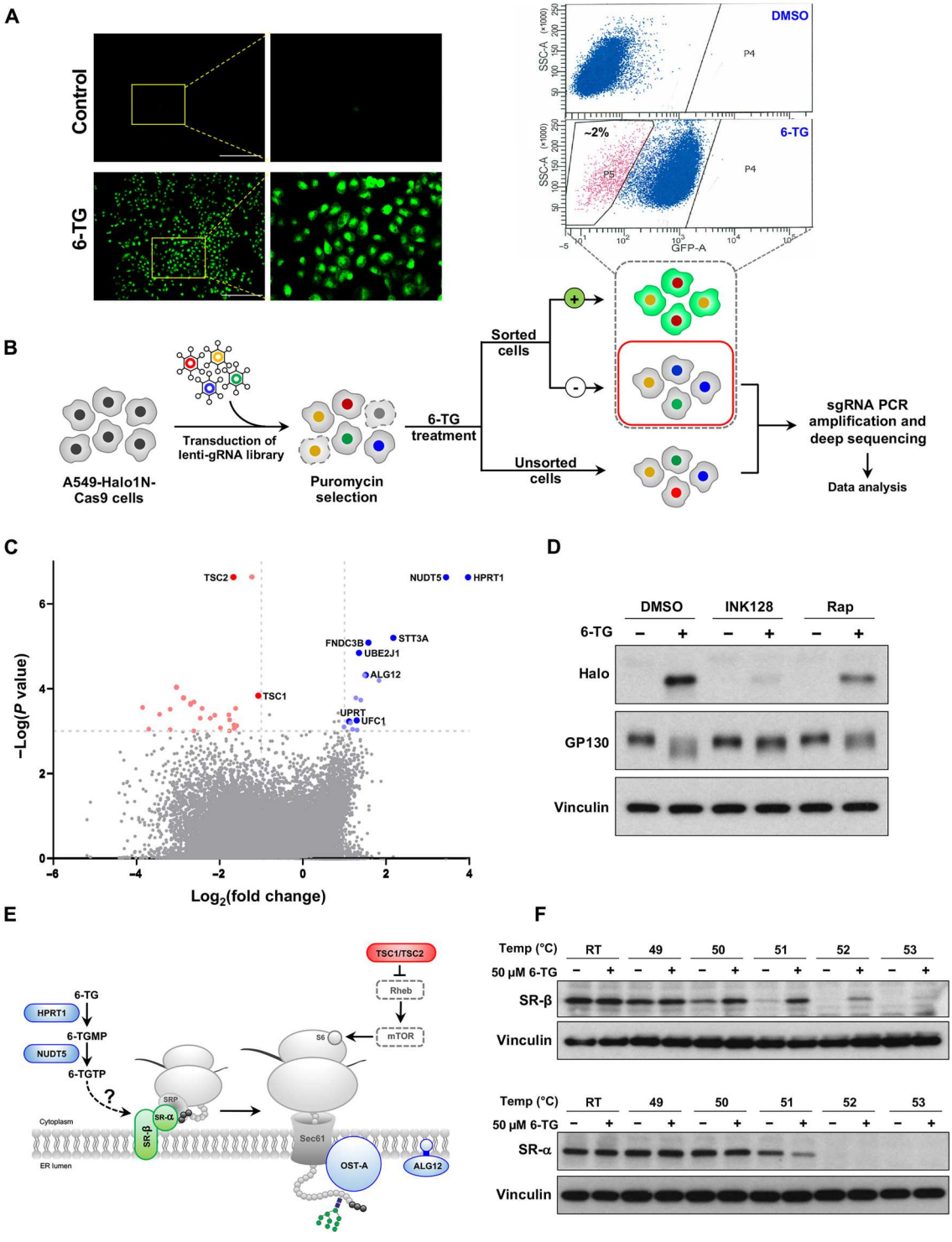

Fig. 2. Whole-genome CRISPR-Cas9 screen to identify the protein target of 6-TG. (**A**) Inhibition of N-glycosylation by 10 μM 6-TG detected by Halo fluorescence. Scale bars, 150 μm. (**B**) Whole-genome CRISPR-Cas9 screening strategy to identify genes that regulate 6-TG activity: following 10 μM 6-TG treatment, ~2% of nonfluorescent cells were sorted from gRNA library–transduced cells and compared to untreated controls. (**C**) Scatterplot showing genes corresponding to gRNAs with positive (blue) or negative (red) $\log_2$ fold changes at a significance level of <0.01. Analysis was performed with three biologically independent samples. (**D**) Effects of mTOR inhibitors [100 nM INK128 and 100 nM rapamycin (Rap)] on Halo1N and gp130 glycosylation in cells treated with 10 μM 6-TG. (**E**) Convergence of significantly over- or underrepresented genes on purine metabolism, translation, and N-glycosylation; associated GTP binding targets are in green. (**F**) Analysis of 6-TG target engagement with SR-α or SR-β using the CTSA. Results are representative of three independent experiments.

glycosylation (Fig. 2E). With this broader view, we focused on the requirement of guanosine triphosphate (GTP) for SRP-SR assembly and ribosome delivery to the translocon. As both components of the SR (SR-α and SR-β) bind GTP (*15*), the SR was investigated as the prime candidate for 6-TG′s effect. Using intact cells for cellular thermal shift assays [CTSAs; (*16*)], we tested whether the SR-α or SR-β subunits are thermostabilized by 6-TG treatment. The results provide evidence for selective target engagement of 6-TG (or its metabolite) with SR-β and show no effect on SR-α (Fig. 2F).

SR-β regulates efficient N-glycosylation

To validate that 6-TG reduces N-glycosylation through an interaction with SR-β, we tested its effects following SR-β KO in A549-Halo1N cells. By fluorescence microscopy, the Halo1N reporter provides spatial resolution to discern whether proteins are nonglycosylated due to dysfunction of the N-glycosylation machinery in the secretory compartment or due to abnormal cytosolic residence. At baseline, SR-β KO reduces translocation of the soluble Halo1N protein into the ER, which can be seen as a nonglycosylated Halo isoform on Western blot (Fig. 3A) and is confirmed by a cytosolic fluorescence pattern revealing a failure to enter the secretory pathway. In addition, we also examined N-glycosylation of gp130 as this transmembrane protein is membrane embedded and its localization and glycosylation are largely unaffected by SR-β KO. We show that 6-TG has no effect on the molecular weight or cellular compartment localization of Halo1N (Fig. 3B) or gp130 (Fig. 3C) in cells with SR-β KO and that 6-TG′s effect on N-glycosylation is rescued by reexpression of a PAM site mutant SR-β (Fig. 3A).

We next asked whether mutagenesis and destabilization of the SR-β GTP binding pocket would alter 6-TG activity. Expression of a C246A mutant not only fully complemented SR-β KO but also reduced the effect of 6-TG on Halo1N and gp130 N-glycosylation (Fig. 3, D and E). 6-TG dose-response experiments showed that C246A increases the median inhibitory concentration (IC_{50}) for the drug′s effect on N-glycosylation as compared to wild-type (WT) SR-β (Fig. 3F). In addition, the C246A mutant showed an overall decrease in thermostability but, unlike the WT SR-β, was not stabilized by 6-TG (Fig. 3H). This result provides further evidence that 6-TG directly interacts with SR-β′s GTP binding site. SR-β functions as a cytosolic ER membrane tether for recruitment of the RNC-SRP complex through interactions with SR-α (*17*), and thus, one possibility is that 6-TG induces transmembrane domain conformational changes to disrupt coordination of the N-glycosylation machinery. However, in parallel experiments with an SR-β transmembrane domain deletion mutant (ΔTM), 6-TG activity was not abolished, thus excluding this possibility (Fig. 3, D and E).

To confirm the role of the GTP binding pocket, we therefore turned our attention to the structure of SR-β crystalized with GTP (*18*), reasoning that structure-guided mutations of the GTP binding pocket should recapitulate the N-glycosylation–deficient phenotype and, if observed, would demonstrate that GTP engagement by SR-β regulates N-glycosylation. We first focused on the oxygen at the guanine 6 position, which is substituted with a sulfur in 6-TG [Fig. 4A and (*19*)]. This oxygen hydrogen bonds with the hydroxyl group of S247, and expression of an S247A mutant revealed a hypoglycosylated Halo1N species by Western blot and fluorescence microscopy (Fig. 4, B and C). The S247 hydroxyl has an intramolecular interaction with the carbonyl oxygen of D183, and similar to S247A, expression of a D183A mutant displayed a mild hypoglycosylation phenotype. Double mutations to D183A and S247A caused a markedly greater N-glycosylation–defective phenotype, determined by complete loss of Halo1N glycosylation on Western blot and secretory compartment fluorescence by microscopy, as well as by inhibition of endogenous gp130 N-glycosylation. 6-TG treatment exacerbated the abnormal N-glycosylation seen with S247A and D183A SR-β mutants but had no further effect on the D183A/S247A double mutant. These data directly demonstrate a heretofore unknown requirement for SR-β in cellular N-glycosylation and indicate that the SR-β GTP binding pocket is a pharmacologically actionable target for inhibition of N-glycosylation.

SR-β regulates assembly of the RNC-SR-translocon-OST supercomplex

But how does SR-β regulate N-glycosylation? The sequon site occupancy data demonstrating a preferential effect of 6-TG on less hydrophobic signal sequences, the identification of SR-β as the 6-TG target, and the partial rescue of N-glycosylation by inhibition of mTOR suggest that robust N-glycosylation requires assembly of an RNC-SR-translocon-OST supercomplex. To test this model, we used coprecipitation of SR-β or the ribosome-interacting OST subunit, RPN1 (*4*), to show that these proteins do indeed associate as a supercomplex under normal conditions (Fig. 4D). In contrast, expression of the SR-β D183A/S247A double mutant reduced coprecipitation of OST subunits (RPN1 and STT3A), but not SR-α. S247A/D183A expression also reduced coprecipitation of SR-α and SR-β with RPN1 (Fig. 4D), while neither STT3A nor STT3B catalytic subunit association was affected. 6-TG treatment also reduced the interaction between SR-β and RPN1, but had no effect on coprecipitation of SR-β and SR-α (fig. S3). These results indicate that a previously unrecognized function of SR-β is to coordinate the formation of an N-glycosylation–competent translocation supercomplex.

DISCUSSION

Defects in N-glycosylation have been attributed to either a failure to synthesize LLOs or functional loss of OST or TRAP complexes in the lumen of the ER (*20*). In this study, we uncover an SR-β–dependent mechanism for OST recruitment that is required for cotranslational N-glycosylation. Both mutation to the SR-β GTP binding site and treatment with the GTP analog 6-TG reduce engagement with the OST and prevent normal N-glycosylation. Quantification of N-glycan site occupancy by mass spectrometry (MS) shows that proteins with less hydrophobic signal sequences, which bind to the SRP with lower affinity (*21*–*23*), have a particularly strong requirement for SR-β. The identification of this subset is consistent with the idea that premature handoff of nascent proteins to a translocon without an associated OST drives the hypoglycosylation phenotype, and is further supported by the observation that inhibition of mTOR and reduced translation corrects this defect. In other words, SR-β allows more time for functional OST supercomplex formation when the signal sequence is less adept at engaging SRP. Given this finding, it is likely that additional cellular mechanisms that increase protein translation rates will also confer SR-β dependence for N-glycosylation, and that proteins with mRNA sequences or amino acid secondary structures that cause ribosomal stalling (*24*, *25*) may be SR-β independent.

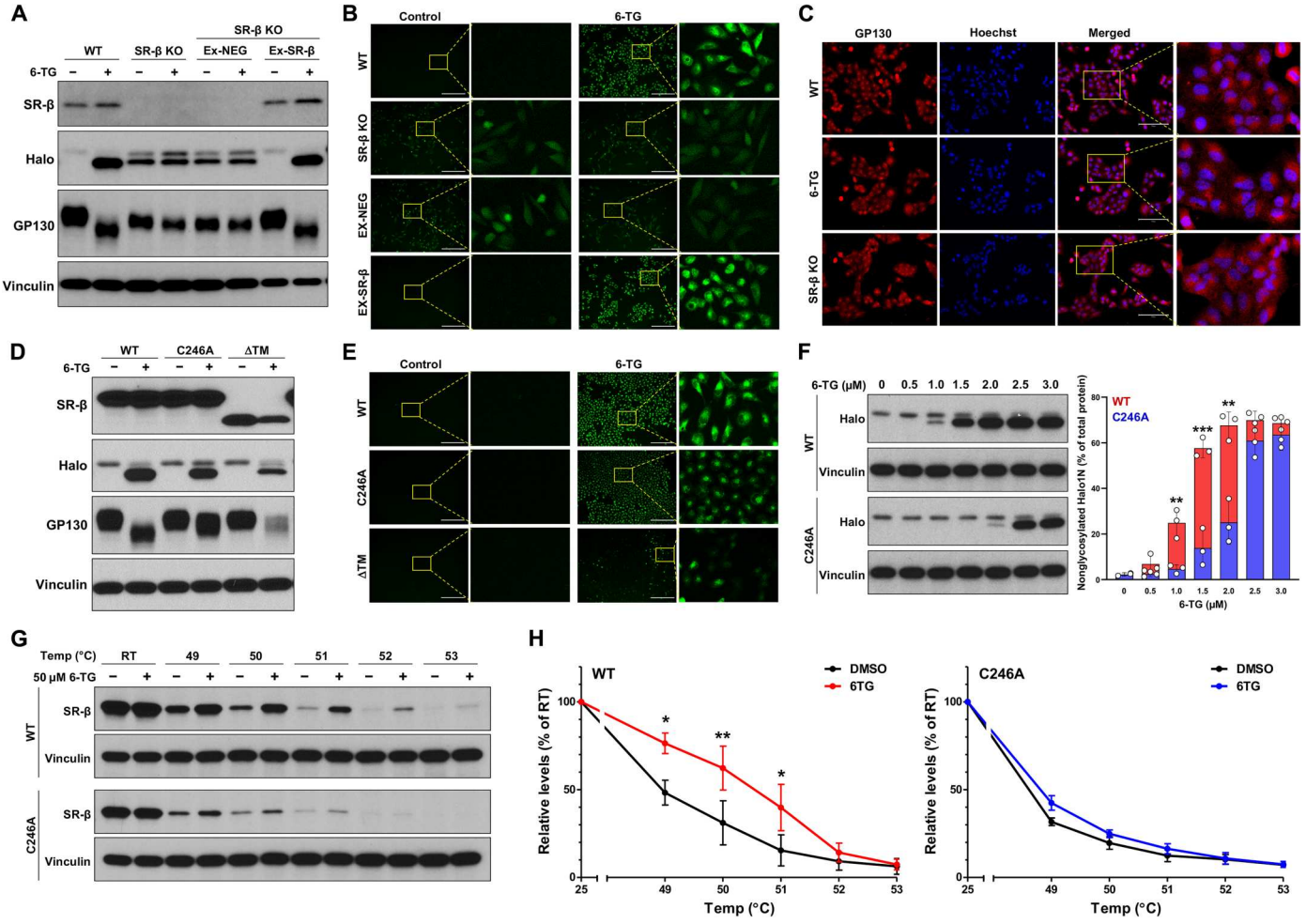

Fig. 3. SR-β is the target of 6-TG. (**A**) Western blot of parental, SR-β KO, empty vector, or PAM site mutated SR-β reexpression with or without 10 μM 6-TG treatment in A549-Halo1N cells. Molecular weight shifts in Halo1N or endogenous gp130 are depicted. (**B**) Fluorescence microscopy for Halo1N with or without 10 μM 6-TG in cell lines described in (A). (**C**) Immunofluorescence for gp130 counterstained with Hoechst in parental and 6-TG–treated cells or with SR-β KO. (**D**) Effects of 6-TG on WT, C246A, or transmembrane domain deleted (ΔTM) SR-β by Western blot or (**E**) fluorescence microscopy. (**F**) Dose-response comparison of 6-TG's effect on N-glycosylation in cells expressing WT or C246A SR-β. Percent of nonglycosylated Halo1N is quantified in the bar graph with significant differences indicated (**$P < 0.01$ and ***$P < 0.001$). (**G**) CTSA comparing 6-TG–induced thermal stabilization for WT or C246A-expressed SR-β. (**H**) Line graphs present the 6-TG–stabilized SR-β level in PAM and C246A cells (*$P < 0.05$ and **$P < 0.01$). All experiments represent data from ≥3 independent experiments. Scale bars, 150 μm (B, C, and E).

The interaction of 6-TG with SR-β provides a chemical biology approach for altering RNC assembly at the translocon and partially blocking N-glycosylation. However, the requirement for conversion of 6-TG by HPRT1 and NUDT5 to an active metabolite (6-TGTP) introduces a substantial time delay for onset of action and limits its use for further dissecting the dynamics of RNC-associated complex assembly. In this regard, development of a small-molecule SR-β inhibitor would be quite useful for further mechanistic studies. The discovery that SR-β dysfunction causes loss of N-glycosylation on a unique subset of proteins and that SR-β is pharmacologically actionable also suggests that SR-β–targeted inhibitors would be of great interest to explore in therapeutic settings, as approaches to partially disrupt N-glycosylation have been identified as potential antiviral (*26*) or antitumor (*8*) strategies.

Through its transmembrane domain, SR-β provides an ER docking mechanism for the RNC that serves as the physical link between signal peptide recognition by the SRP and subsequent ribosome positioning on the translocon achieved through SRP-SR association (*27*). It is also understood that binding of GTP to SR-β is required for heterodimerization with SR-α (*28*); however, SR-β GTP binding domain mutations did not alter coprecipitation with SR-α and indicate that SR-β's role in coordinating the cell's translocation machinery is beyond that of simple membrane localization. Our data support a model where SR-β also provides a timing mechanism that allows for supercomplex assembly before protein translocation and N-glycosylation (Fig. 4E), a pause conceptually similar to the RNC-induced delay of SRP and SR guanosine triphosphatase (GTPase) activation that allows time for RNC targeting to the translocon (*29*).

The recruitment of OST to the assembling RNC-SR-translocon complex provides further insight into the events surrounding nascent chain handover to the translocon, which occurs concurrently with SRP and SR dissociation from the RNC (*2*, *30*), and allows cotranslational translocation across the ER to initiate.

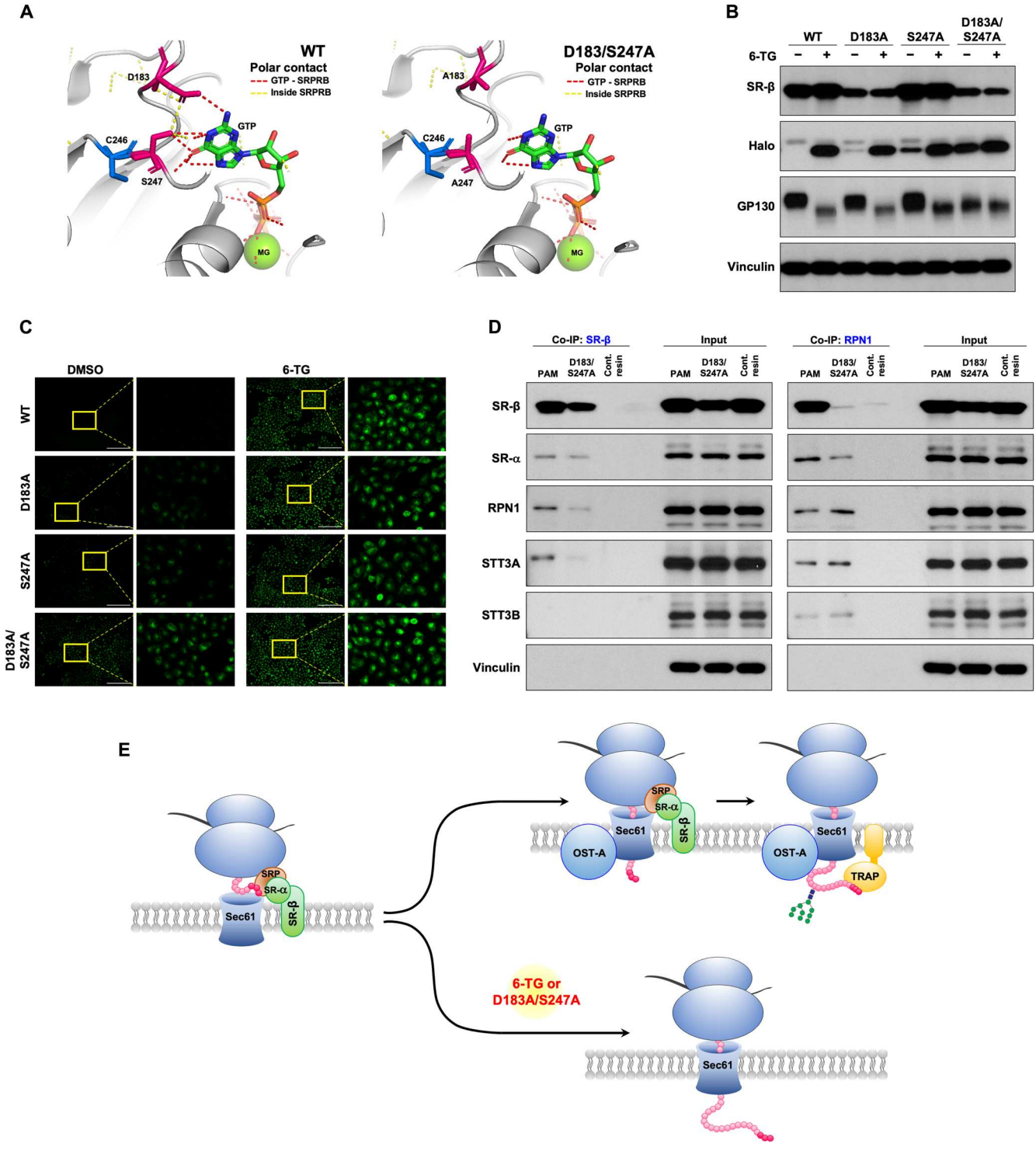

Fig. 4. SR-β regulates assembly of the glycosylation-competent translocon. (**A**) Modeling of SR-β binding to GTP using structures from Protein Data Bank #7NFX (*19*) and predicted interactions of D183A and S247A with GTP. (**B**) Western blot and (**C**) microscopy of WT, D183A, S247A, or D183A/S247A double mutant SR-β with or without 10 μM 6-TG treatment. Scale bars, 150 μm. (**D**) Coimmunoprecipitation of SRP, ribosome, or OST subunits with anti–SR-β or anti-RPN1. Data are representative of three independent experiments. (**E**) Illustration of SR-β's role in coordinating proficient N-glycosylation or impairment of N-glycosylation by 6-TG treatment or SR-β mutation.

Because of its transitory nature, the components and structure of this complex have remained elusive. The demonstration that pharmacologic and genetic manipulation of SR-β reduces its association with components of the multisubunit OST complex indicates that the OST is part of the in situ RNC-SR handover complex and that precise assembly of this supercomplex is essential for cotranslational N-glycosylation.

MATERIALS AND METHODS

Cell culture

A549, FaDu, HCT 116, human embryonic kidney (HEK)–293, and HEK-293T cell lines were purchased from the American Type Culture Collection (Rockville, MD). The A549 cells were cultured in RPMI (Gibco, Life Technologies, Grand Island, NY); FaDu, HEK-293, and HEK-293T cells were cultured in Dulbecco′s modified Eagle medium (Gibco); and HCT 116 cells were cultured in McCoy′s 5a (Gibco) Medium Modified supplemented with 10% fetal bovine serum (Gibco) and penicillin and streptomycin (Gibco) in a humidified incubator with 5% CO_2. Cells were kept in culture no more than 6 months after resuscitation from the original stocks. The A549 and HEK-293 Cas9-expressing cells were generated via lentiviral transduction using virus produced from the lentiCas9-Blast (Addgene, 52962), psPAX2 packaging, and pMD2.GVG envelope plasmids (*6*). Cells with Halo1N were grown in G418 supplemented medium.

A549 FNDC3B KO, A549 UBE2J1 KO, and A549 SR-β KO cells were generated from A549 cells expressing Cas9, followed by lentiviral expression of gene-targeting gRNAs (table S6). Target gene KO or knockdown was confirmed by Western blot and DNA sequencing. For reexpression of SR-β (EX-A3210-M68) or an empty vector control (EX-NEG-M68), OmicsLink plasmids were purchased from GeneCopoeia (Rockville, MD). The Cas9 gRNA PAM binding site for SR-β (which enables SR-β expression by reducing Cas9 nuclease activity) was mutated from CGG to CGA, and this plasmid was used as a template for all SR-β mutants. SR-β mutations were constructed using the QuikChange II XL Site-Directed Mutagenesis Kit (200522, Agilent, Santa Clara, CA). The oligonucleotides for site-directed mutagenesis are listed in table S6. Mutated SR-β plasmid was digested and inserted into pLV-EF1a-IRES-Puro (Addgene, 85132). Lentivirus carrying mutated *SRPRB* gene was then transduced into the A549 SR-β KO cells at a multiplicity of infection (MOI) of ~0.5.

Drug screening

The HTS approach using the bioluminescent reporter in D54-expressing ER-LucT or LucT cells has been previously described (*8*, *9*). Briefly, primary screening is aimed to detect the deficiency of N-linked glycan site occupancy in an ER-translated luciferase protein with three N-linked glycosylation consensus sequons (ER-LucT). For the secondary false-positive screen, LucT without the ER translation sequence is used to identify false positives. The methodology for the initial primary (D54 ER-LucT), secondary false-positive (D54 LucT), and tertiary (luciferase inhibition) screens as well as toxicity assays with CellTiter Glo are deposited in PubChem (AID 588693). The activity of small molecules on inhibition of N-glycosylation was evaluated by Western blot analysis using Halo3N (*10*). NGI-1 and tunicamycin were used as positive controls.

CRISPR-Cas9 screening combined FACS

The hGeCKO library (Addgene, 1000000049, hGeCKOa and hGeCKOb) was generated as previously described (*6*). For each of the three biologically independent replicates, 1×10^8 A549-Halo1N-Cas9 cells were infected with lentiGuide-Puro from the hGeCKO library at an MOI of 0.3 and selected with puromycin at 2 μg/ml for 10 days. After puromycin selection, the cultures were treated with 10 μM 6-TG for 24 hours, trypsinized, treated with the HaloTag ligand (1:1000; Promega, G2801) for 1 hour at 37°C, and then sorted by flow cytometry for the negative Halo signal population. Unsorted cells were treated in the same manner and used as a control.

Genomic DNA sequencing and analysis

The gRNA sequencing and analysis have been previously described (*6*). Briefly, genomic DNA from the cells was isolated using QIAamp DNA columns (Qiagen, Hilden, Germany), and gRNA sequences were amplified and barcoded for next-generation sequencing using two-step polymerase chain reaction (PCR). All PCRs were performed using Phusion Flash High-Fidelity Master Mix (Thermo Fisher Scientific, F548L). Sequencing was performed with Illumina HiSeq and 75–base pair single-end reads at the Yale Center for Genome Analysis. Reads were aligned to index sequences using the Bowtie aligner, and a maximum of one mismatch was allowed in the 20–base pair gRNA sequence. The number of uniquely aligned reads for each library sequence was calculated after alignment for each of three biologically independent replicates.

Glycoproteomics for N-linked glycosylation site occupancy

Glycopeptides were enriched for MS and analyzed by liquid chromatography–tandem mass spectrometry (LC-MS/MS) as described previously (*11*) with minor modifications. For these experiments, HeLa cells were treated with 6-TG for 24 hours and compared to controls. The isolated glycopeptide mixtures were prepared and analyzed by LC-MS/MS in four experiments (control versus 6-TG) or five experiments (control versus NGI-1) to obtain glycosylation site occupancy for ~800 sites identified in two or more LC-MS/MS experiments. The $\Delta\log_2$ values were calculated for spectra and then averaged for those peptides, where multiple quantified spectra were obtained in a single LC-MS/MS experiment. The SILAC datasets for control versus 6-TG and control versus NGI-1 are tabulated in tables S1 and S2, respectively.

Fluorophore-assisted carbohydrate electrophoresis

HEK-293 cells were treated with or without 10 μM 6-TG for 24 hours before isolation of LLO, and the prevalence of individual species was determined by fluorophore-assisted carbohydrate electrophoresis (FACE), as described previously (*8*).

Cellular thermal shift assay

CTSA was performed in A549 cells with SR-β KO and complementation with either a PAM site mutant of SR-β or individual mutants as described. Briefly, cells were treated with 100 μM 6-TG for 3 hours. After treatment, the cells were harvested and resuspended in phosphate-buffered saline (PBS) containing protease inhibitor with/without 100 μM 6-TG. Cells (2×10^6) in 100 μl of medium were subjected to thermal treatment for 3 min and continued for 3-min incubation at room temperature. The protein levels were then determined by Western blot (*16*).

SDS-PAGE and Western blot

Cells were lysed with buffer containing protease and phosphatase inhibitors. Following cell lysis, proteins were separated by SDS–polyacrylamide gel electrophoresis (SDS-PAGE) and transferred onto a nitrocellulose membrane. The following primary antibodies were used: anti-ALG12 (1:1000; PA5-50316, Invitrogen), anti-FNDC3B (1:1000; B-1, sc-393997, Santa Cruz Biotechnology, Dallas, TX), anti-GP130 (1:1000; M-20, sc-656, Santa Cruz Biotechnology), anti-HaloTag (1:3000; G9281, Promega, Madison, WI), anti-HPRT (1:1000; F-4, sc-376922, Santa Cruz Biotechnology), anti-phospho-RPS6 S253/236 (1:1000; 2211, Cell Signaling Technology, Danvers, MA), anti-RPN1 (1:500; 12894-1-AP, Proteintech, Rosemont, IL), anti-RPS6 kinase (1:1000; 54D2, 2317, Cell Signaling Technology), anti-Sec61A1 (1:500; D7Q6V, 14868, Cell Signaling Technology), anti–SR-α (1:1000; PA5-28295, Invitrogen), anti–SR-β (1:500; 14636-1-AP, Proteintech), anti-SSR2 (1:500; 10278-1-AP, Proteintech), anti-STT3A (1:500; 12034-1-AP, Proteintech), anti-STT3B (1:500; 15323-1-AP, Proteintech), anti-UBE2J1 (1:800; B-6, sc-377002, Santa Cruz Biotechnology), and anti-vinculin (1:2000; E1E9V, 13901, Cell Signaling Technology). The immunoblotting reactivity was detected using the ECL Western Blotting Detection Reagents (GE Healthcare).

HaloTag ligand detection

Loss of glycosylation on Halo1N protein was evaluated by fluorescent microscopy using the HaloTag Oregon Green Ligand (Promega, Madison, WI) with an Evos M5000 microscope (Thermo Fisher Scientific) and ×200 magnification. Cells were incubated with 1:1000 HaloTag ligand in culture medium at 37°C for 20 min after the specified experimental conditions as described previously (*6*). Excess ligand was washed twice with PBS, and unbound ligand was then washed out with culture medium at 37°C for 30 min.

Coimmunoprecipitation

Protein-protein interactions were determined using the Pierce Coimmunoprecipitation Kit (Pierce Biotechnology) according to the manufacturer′s protocol. Briefly, 5 μg of antibodies was immobilized with AminoLink Plus Coupling Resin, and a total of 2 mg of whole-cell lysate was incubated overnight with the resin-antibody complex at 4°C. Protein-bound antibodies were eluted and solubilized in Lane Marker Sample Buffer before they were subjected to SDS-PAGE. The lysate incubated with antibody-control agarose resin complex was used as the negative control.

Statistical analysis

Statistical analysis not described above was determined using Student′s *t* test (GraphPad Prism 8.0 software, GraphPad Software Inc., La Jolla, CA), and $P < 0.05$ was considered statistically significant.

Supplementary Materials

This PDF file includes:
Figs. S1 to S3
Legends for tables S1 and S2
Tables S3 to S6

Other Supplementary Material for this manuscript includes the following:
Tables S1 and S2

View/request a protocol for this paper from *Bio-protocol*.

REFERENCES AND NOTES

1. C. Ruiz-Canada, D. J. Kelleher, R. Gilmore, Cotranslational and posttranslational N-glycosylation of polypeptides by distinct mammalian OST isoforms. *Cell* **136**, 272–283 (2009).
2. A. Jomaa, S. Eitzinger, Z. Zhu, S. Chandrasekar, K. Kobayashi, S. O. Shan, N. Ban, Molecular mechanism of cargo recognition and handover by the mammalian signal recognition particle. *Cell Rep.* **36**, 109350 (2021).
3. K. Kobayashi, A. Jomaa, J. H. Lee, S. Chandrasekar, D. Boehringer, S.-O. Shan, N. Ban, Structure of a prehandover mammalian ribosomal SRP.SRP receptor targeting complex. *Science* **360**, 323–327 (2018).
4. K. Braunger, S. Pfeffer, S. Shrimal, R. Gilmore, O. Berninghausen, E. C. Mandon, T. Becker, F. Förster, R. Beckmann, Structural basis for coupling protein transport and N-glycosylation at the mammalian endoplasmic reticulum. *Science* **360**, 215–219 (2018).
5. A. S. Ramirez, J. Kowal, K. P. Locher, Cryo-electron microscopy structures of human oligosaccharyltransferase complexes OST-A and OST-B. *Science* **366**, 1372–1375 (2019).
6. C. Phoomak, W. Cui, T. J. Hayman, S.-H. Yu, P. Zhao, L. Wells, R. Steet, J. N. Contessa, The translocon-associated protein (TRAP) complex regulates quality control of N-linked glycosylation during ER stress. *Sci. Adv.* **7**, eabc6364 (2021).
7. A. Takatsuki, G. Tamura, Tunicamycin, a new antibiotic. II. Some biological properties of the antiviral activity of tunicamycin. *J. Antibiot. (Tokyo)* **24**, 224–231 (1971).
8. C. Lopez-Sambrooks, S. Shrimal, C. Khodier, D. P. Flaherty, N. Rinis, J. C. Charest, N. Gao, P. Zhao, L. Wells, T. A. Lewis, M. A. Lehrman, R. Gilmore, J. E. Golden, J. N. Contessa, Oligosaccharyltransferase inhibition induces senescence in RTK-driven tumor cells. *Nat. Chem. Biol.* **12**, 1023–1030 (2016).
9. D. C. Bennett, J. Charest, K. Sebolt, M. Lehrman, A. Rehemtulla, J. N. Contessa, High-throughput screening identifies aclacinomycin as a radiosensitizer of EGFR-mutant non-small cell lung cancer. *Transl. Oncol.* **6**, 382–391 (2013).
10. N. Rinis, J. E. Golden, C. D. Marceau, J. E. Carette, M. C. Van Zandt, R. Gilmore, J. N. Contessa, Editing N-glycan site occupancy with small-molecule oligosaccharyltransferase inhibitors. *Cell Chem. Biol.* **25**, 1231–1241 e4 (2018).
11. N. A. Cherepanova, S. V. Venev, J. D. Leszyk, S. A. Shaffer, R. Gilmore, Quantitative glycoproteomics reveals new classes of STT3A- and STT3B-dependent N-glycosylation sites. *J. Cell Biol.* **218**, 2782–2796 (2019).
12. S. Liao, M. Tammaro, H. Yan, Enriching CRISPR-Cas9 targeted cells by co-targeting the HPRT gene. *Nucleic Acids Res.* **43**, e134 (2015).
13. K. Inoki, Y. Li, T. Zhu, J. Wu, K.-L. Guan, TSC2 is phosphorylated and inhibited by Akt and suppresses mTOR signalling. *Nat. Cell Biol.* **4**, 648–657 (2002).
14. C. P. Walczak, D. E. Leto, L. Zhang, C. Riepe, R. Y. Muller, P. A. DaRosa, N. T. Ingolia, J. E. Elias, R. R. Kopito, Ribosomal protein RPL26 is the principal target of UFMylation. *Proc. Natl. Acad. Sci. U.S.A.* **116**, 1299–1308 (2019).
15. J. D. Miller, H. Wilhelm, L. Gierasch, R. Gilmore, P. Walter, GTP binding and hydrolysis by the signal recognition particle during initiation of protein translocation. *Nature* **366**, 351–354 (1993).
16. R. Jafari, H. Almqvist, H. Axelsson, M. Ignatushchenko, T. Lundbäck, P. Nordlund, D. M. Molina, The cellular thermal shift assay for evaluating drug target interactions in cells. *Nat. Protoc.* **9**, 2100–2122 (2014).
17. J. D. Miller, S. Tajima, L. Lauffer, P. Walter, The β subunit of the signal recognition particle receptor is a transmembrane GTPase that anchors the alpha subunit, a peripheral membrane GTPase, to the endoplasmic reticulum membrane. *J. Cell Biol.* **128**, 273–282 (1995).
18. T. Schwartz, G. Blobel, Structural basis for the function of the β subunit of the eukaryotic signal recognition particle receptor. *Cell* **112**, 793–803 (2003).
19. J. H. Lee, A. Jomaa, S. Chung, Y.-H. H. Fu, R. Qian, X. Sun, H.-H. Hsieh, S. Chandrasekar, X. Bi, S. Mattei, D. Boehringer, S. Weiss, N. Ban, S.-O. Shan, Receptor compaction and GTPase rearrangement drive SRP-mediated cotranslational protein translocation into the ER. *Sci. Adv.* **7**, eabg0942 (2021).
20. D. J. Lefeber, H. H. Freeze, R. Steet, T. Kinoshita, Congenital disorders of glycosylation, in *Essentials of Glycobiology*, A. Varki, R.D. Cummings, J.D. Esko, P. Stanley, G.W. Hart, M. Aebi, D. Mohnen, T. Kinoshita, N. H. Packer, J. H. Prestegard, R. L. Schnaar, P. H. Seeberger, Eds. (Cold Spring Harbor Laboratory Press, ed. 4, 2022), pp. 599–614.
21. C. Y. Janda, J. Li, C. Oubridge, H. Hernández, C. V. Robinson, K. Nagai, Recognition of a signal peptide by the signal recognition particle. *Nature* **465**, 507–510 (2010).
22. I. Nilsson, P. Lara, T. Hessa, A. E. Johnson, G. von Heijne, A. L. Karamyshev, The code for directing proteins for translocation across ER membrane: SRP cotranslationally recognizes specific features of a signal sequence. *J. Mol. Biol.* **427**, 1191–1201 (2015).

23. A. M. Liaci, F. Förster. Data Archiving and Networked Services (DANS): The Hague, The Netherlands, Mendeley Data (2021).
24. J.-R. Yang, X. Chen, J. Zhang, Codon-by-codon modulation of translational speed and accuracy via mRNA folding. *PLOS Biol.* **12**, e1001910 (2014).
25. S. Kanda, K. Yanagitani, Y. Yokota, Y. Esaki, K. Kohno, Autonomous translational pausing is required for XBP1u mRNA recruitment to the ER via the SRP pathway. *Proc. Natl. Acad. Sci. U.S.A.* **113**, E5886–E5895 (2016).
26. A. S. Puschnik, C. D. Marceau, Y. S. Ooi, K. Majzoub, N. Rinis, J. N. Contessa, J. E. Carette, A small-molecule oligosaccharyltransferase inhibitor with pan-flaviviral activity. *Cell Rep.* **21**, 3032–3039 (2017).
27. W. Song, D. Raden, E. C. Mandon, R. Gilmore, Role of Sec61alpha in the regulated transfer of the ribosome-nascent chain complex from the signal recognition particle to the translocation channel. *Cell* **100**, 333–343 (2000).
28. G. Bacher, M. Pool, B. Dobberstein, The ribosome regulates the GTPase of the β-subunit of the signal recognition particle receptor. *J. Cell Biol.* **146**, 723–730 (1999).
29. X. Zhang, C. Schaffitzel, N. Ban, S.-o. Shan, Multiple conformational switches in a GTPase complex control co-translational protein targeting. *Proc. Natl. Acad. Sci. U.S.A.* **106**, 1754–1759 (2009).
30. T. A. Fulga, I. Sinning, B. Dobberstein, M. R. Pool, SRβ coordinates signal sequence release from SRP with ribosome binding to the translocon. *EMBO J.* **20**, 2338–2347 (2001).

Acknowledgments: We wish to acknowledge N. Gao for contributions in the analysis of LLOs. We also acknowledge the following centers for their assistance: the Yale Center for Genome Analysis for their next-generation sequencing and bioinformatics pipelines, the Keck DNA Sequencing Facility at Yale for their Sanger sequencing service, the Yale Flow Cytometry Core for cell sorting experiment, and the UMass Mass Spectrometry facility. **Funding:** This work was supported by NIH grants R01 CA240418, R01 GM127383, and R03 DA033178 (to J.N.C.); R01 GM43768 (to R.G.); and R01 GM038545 (to M.L.). **Author contributions:** Conceptualization: C.P., M.L., R.G., and J.N.C. Methodology: C.P., N.R., M.B., D.B., S.S., S.A.S., and J.N.C. Investigation: C.P., N.R., M.B., D.B., S.S., S.A.S., and J.N.C. Visualization: C.P. and J.N.C. Supervision: M.L., R.G., and J.N.C. Writing—original draft: C.P. and J.N.C. Writing—review and editing: C.P., M.L., R.G., and J.N.C. **Competing interests:** The authors declare that they have no competing interests. **Data and materials availability:** All data needed to evaluate the conclusions in the paper are present in the paper and/or the Supplementary Materials.

Submitted 8 September 2022
Accepted 14 February 2023
Published 15 March 2023
10.1126/sciadv.ade8079